

# Investigation of thin perovskite layers between cathode and doped ceria used as buffer layer in solid oxide fuel cells

Aleksander Chrzan · Jakub Karczewski · Maria Gazda ·  
Dagmara Szymczewska · Piotr Jasinski

Received: 12 December 2014 / Revised: 2 March 2015 / Accepted: 4 March 2015 / Published online: 24 March 2015  
© The Author(s) 2015. This article is published with open access at Springerlink.com

**Abstract** In this paper, thin perovskite layers between cathode material of solid oxide fuel cells and gadolinia-doped ceria buffer layer are investigated. Thin layers made of  $\text{LaNi}_{0.6}\text{Fe}_{0.4}\text{O}_{3-\delta}$  (LNF),  $\text{La}_{0.6}\text{Sr}_{0.4}\text{Co}_{0.2}\text{Fe}_{0.8}\text{O}_{3-\delta}$  (LSCF), or  $\text{SrTi}_{0.65}\text{Fe}_{0.35}\text{O}_{3-\delta}$  (STF) were symmetrically deposited by spin coating method from metallo-organic polymer precursors on a  $\text{Ce}_{0.8}\text{Gd}_{0.2}\text{O}_{2-\delta}$  (CGO) substrate. Porous and about 40- $\mu\text{m}$ -thick LNF cathodes were deposited on both sides of the substrate and sintered at 1100 °C. Different thicknesses of the thin perovskite layer were investigated in order to find the most effective one and to better understand its influence on the cathode/electrolyte interface. It was found that approximately 150 nm LNF or LSCF layer is sufficient to minimize interface resistance and improve cathode reproducibility. It was concluded that the thin perovskite layer increases contact area and improves the oxygen ion transport between the cathode and electrolyte without influencing the oxygen reduction reaction mechanism.

**Keywords** Perovskite layer · Thin film · Cathode · Solid oxide fuel cell

## Introduction

Fuel cells are devices that directly convert chemical energy into electricity. As a result, they are not limited by the

Carnot cycle, therefore can achieve high efficiency. Also, utilization of hydrogen as a fuel implicates the lack of  $\text{CO}_2$  and other pollutant emission. The ones of the most promising types of fuel cells are solid oxide fuel cells (SOFC). They have high efficiency, they can be fueled by either hydrogen or hydrocarbons and do not include any moving parts, which might reduce durability [1]. SOFCs usually consist of ceramic or cermet, porous electrodes separated by a dense, oxide-ion conducting ceramic membrane, usually made of yttria-stabilized zirconia (YSZ). Using such materials implies the main SOFC feature—high-temperature operation. Traditional, high-temperature fuel cells provide sufficient power density above 800 °C. It is crucial to lower operation temperature to medium-temperature range (600–800 °C). This enables usage of less expensive materials, lowers thermal stress, shortens start-up and shut-down time, and reduces number of possible unwanted chemical reactions between fuel cell components [2]. On the other hand, lower temperature decreases both conductivity and catalytic activity of fuel cells, especially cathodes [3, 4]. Therefore, there is ongoing search for novel cathode materials exhibiting an improved performance at temperatures below 800 °C [4–6]. Apart from an appropriate chemical composition of the cathode, it is also important to properly adjust the microstructure, especially of the cathode/electrolyte interface [7–10]. As a result, it became a common practice to incorporate of at least 10- $\mu\text{m}$ -thick cathode functional layer, which has a finer microstructure than a cathode current collector layer [11]. The justifiability of such a layer was also proven theoretically [12]. Recently, much thinner functional layers between the cathode/electrolyte were found to improve fuel cell performance. Such a layer has been prepared by dip-coating (2  $\mu\text{m}$  thick) by Rieu [13] and by screen printing (5  $\mu\text{m}$  thick) by Woolley [14], and it decreased polarization resistance of a  $\text{La}_2\text{NiO}_{4+\delta}$

A. Chrzan (✉) · D. Szymczewska · P. Jasinski  
Faculty of Electronics, Telecommunications and Informatics, Gdansk  
University of Technology, Narutowicza 11/12,  
80-233 Gdansk, Poland  
e-mail: aleksander.chrzan@eti.pg.gda.pl

J. Karczewski · M. Gazda  
Faculty of Applied Physics and Mathematics, Gdansk University of  
Technology, Narutowicza 11/12, 80-233 Gdansk, Poland

electrode. Hildenbrand reported an improvement of the cathode/electrolyte interface for  $\text{La}_{0.6}\text{Sr}_{0.4}\text{Co}_{0.2}\text{Fe}_{0.8}\text{O}_{3-\delta}$  (LSCF) and  $\text{La}_2\text{NiO}_{4+\delta}$  cathodes using a thin dense layer obtained by pulsed laser deposition [15, 16]. Recently, Dumaisnil investigated a spin-coated 700-nm-thick LSCF layer between a  $\text{Ce}_{0.9}\text{Gd}_{0.1}\text{O}_{2-\delta}$  electrolyte and an LSCF cathode [17]. Previous studies focused on cathodes with high ionic conductivity and dense layers made of the same material. None of primary electronically conductive cathode materials has been studied so far. Therefore, it is substantial to establish if the thin perovskite layer can also improve properties of a cell with the predominantly electronic conducting cathode. This issue was addressed in this paper. Namely, the  $\text{LaNi}_{0.6}\text{Fe}_{0.4}\text{O}_{3-\delta}$  (LNF) cathodes with the thin perovskite layers of different types of conductivity, i.e., LNF, LSCF, and  $\text{SrTi}_{0.65}\text{Fe}_{0.35}\text{O}_{3-\delta}$  (STF), were investigated. LNF is a mixed ionic-electronic conductor with relatively low ionic conductivity and a promising cathode or current collector material due to a moderate stability in the presence of chromia [18, 19]. LSCF is a state-of-the-art mixed ionic-electronic conductor [4, 5]. STF is a much weaker electronic conductor but exhibits higher ionic conductivity and the order of magnitude higher surface exchange coefficient [20]. Table 1 lists ionic and electronic conductivities of these perovskites at 800 °C.

Thin perovskite layers were fabricated using spin coating of a metallo-organic precursor. This method is well suited for a large-scale production and enables an easy control over the layer thickness. The thickness of the thin perovskite layer was also altered, i.e., from about 25 to 400 nm, in order to find the most efficient one. To deposit and investigate thin perovskite layers, a  $\text{Ce}_{0.8}\text{Gd}_{0.2}\text{O}_{2-\delta}$  (CGO) support was used. CGO is often used as an electrolyte instead of YSZ [26]. It is also employed as a buffer layer preventing reactions between zirconium from YSZ electrolyte and strontium or lanthanum from certain cathodes, for example LNF [27]. Thin perovskite layers made of LNF and STF were studied for the first time.

## Experimental

In order to evaluate the cathode/buffer layer interface, symmetrical cells with two LNF electrodes were prepared on a gadolinia-doped ceria (CGO) substrate. The substrates were prepared from the CGO powder (GDC-20 K, Daiichi Kigenso Kagaku Kogyo), which was uniaxially pressed under a pressure of 100 MPa and sintered at 1350 °C for 4 h. Obtained pellets were 1 mm thick and had a diameter of 13 mm. The measured density of pellets was 99 % of the theoretical, which was enough to prevent spin-coated precursor from infiltrating the substrate.

Three different thin perovskite layers, i.e.,  $\text{LaNi}_{0.6}\text{Fe}_{0.4}\text{O}_{3-\delta}$  (LNF),  $\text{La}_{0.6}\text{Sr}_{0.4}\text{Co}_{0.2}\text{Fe}_{0.8}\text{O}_{3-\delta}$  (LSCF), and  $\text{SrTi}_{0.65}\text{Fe}_{0.35}\text{O}_{3-\delta}$  (STF), were prepared by spin coating of

**Table 1** Electronic and ionic conductivities at 800 °C of perovskites used for thin film fabrication

Material	$\sigma_{\text{el}}$ [ $\text{S cm}^{-1}$ ]	$\sigma_{\text{ion}}$ [ $\text{S cm}^{-1}$ ]	Ref.
$\text{LaNi}_{0.6}\text{Fe}_{0.4}\text{O}_{3-\delta}$	200–700	$7 \times 10^{-5}$	[21–23]
$\text{La}_{0.6}\text{Sr}_{0.4}\text{Co}_{0.2}\text{Fe}_{0.8}\text{O}_{3-\delta}$	280–330	$8 \times 10^{-3}$	[4, 5, 24, 25]
$\text{SrTi}_{0.65}\text{Fe}_{0.35}\text{O}_{3-\delta}$	0.99	$3.5 \times 10^{-2}$	[20]

polymer precursors. The precursors were prepared by a modified Pechini method [28] by mixing ethylene glycol, citrate acid, and appropriate metal nitrates ( $\text{La}(\text{NO}_3)_3 \times 6\text{H}_2\text{O}$ ,  $\text{Ni}(\text{NO}_3)_2 \times 6\text{H}_2\text{O}$ ,  $\text{Fe}(\text{NO}_3)_3 \times 9\text{H}_2\text{O}$ ,  $\text{Sr}(\text{NO}_3)_2$ ,  $\text{Co}(\text{NO}_3)_2 \times 6\text{H}_2\text{O}$ ), or titanium(IV)butoxide (all Sigma-Aldrich) using molar ratio of 40:2.2:1, respectively. In order to increase wetting properties and control viscosity, 2-ethoxyethanol was added to the solution. The precursors were spin coated on polished CGO pellets for 2 min at 2500 rpm. After every deposition samples were fired at 500 °C on a hot plate. At this point, the deposited films were dense, and their thicknesses were calculated based on a sample weight change and later confirmed by a SEM examination. Each of the spin coating process (deposition of about 30  $\mu\text{l}$  of precursor) produced layer approximately 24 nm thick for LNF and 27 nm thick for LSCF and STF. The precursor compositions and the spin coating parameters were chosen experimentally based on film morphology.

Round cathodes with a diameter of 7 mm were brush painted on the thin perovskite layers using a  $\text{LaNi}_{0.6}\text{Fe}_{0.4}\text{O}_{3-\delta}$  paste obtained from *Energy Research Centre of the Netherlands, Petten*. To obtain the reproducible and flat cathode, the painting was repeated three times. The amount of paste was controlled by weight in order to deposit approximately 40- $\mu\text{m}$ -thick layers. Cathodes were sintered at 1100 °C for 2 h. Lower sintering temperatures provided layers which could be easily delaminated. Platinum current collector layers, about 5  $\mu\text{m}$  thick, were brush painted (ESL 5542) on LNF cathodes and sintered at 900 °C for 2 h. Schematic representation of a sample is shown in Fig. 1. In order to determine the reproducibility of the results, each arrangement has been prepared at least three times.

Structural information was obtained using X-ray diffraction (Philips X'Pert Pro) with Cu K $\alpha$  radiation at room temperature. Sample morphology was determined by scanning electron microscopy (SEM, Quanta 250 FEI) and atomic

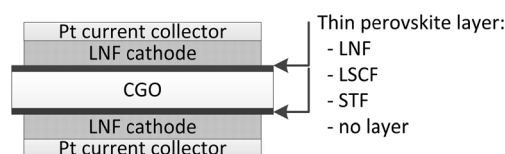


**Fig. 1** Schematic representation of symmetrical cells

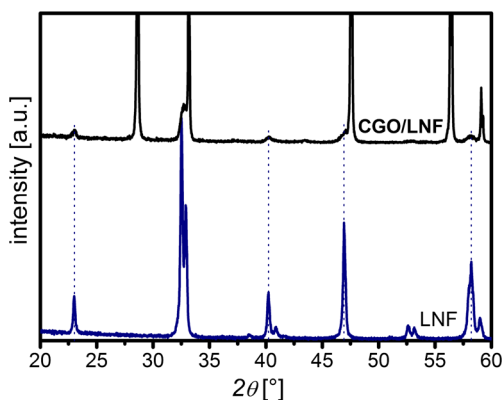


**Fig. 2** XRD patterns of the bulk LNF and the LNF thin layer deposited on a CGO substrate and annealed at 1100 °C (dotted vertical lines match the peaks corresponding to the bulk and thin layer LNF)

force microscopy (AFM, Nanosurf EasyScan II) in contact mode. An AFM micrograph analysis was performed in Gwyddion program. Pellet density was measured using a fluid displacement method with kerosene as a working liquid. Symmetrical cells were characterized by the electrochemical impedance spectroscopy (EIS) using Solartron SI 1260 impedance analyzer coupled with SI 1287 electrochemical interface. The measurements were carried out in dry air in frequency range from 0.5 Hz to 1 MHz and amplitude of 10 mV. The spectra were collected in the temperature range from 800 to 600 °C with 50 °C step.

## Results and discussion

### Structural characterization of prepared films

Thin perovskite layers spin coated on CGO substrates without depositing LNF cathode were investigated using XRD analysis in order to analyze their structure. The XRD measurements

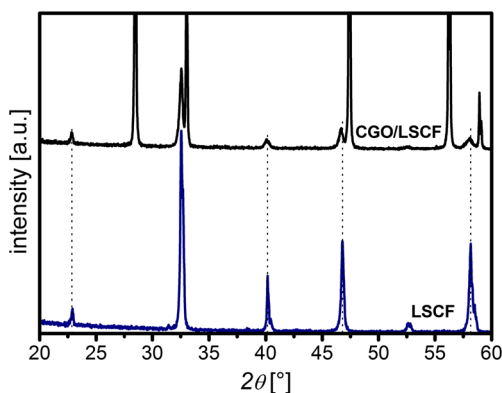


**Fig. 3** XRD patterns of the bulk LSCF and the LSCF thin layer deposited on a CGO substrate and annealed at 1100 °C (dotted vertical lines match the peaks corresponding to the bulk and thin layer LSCF)

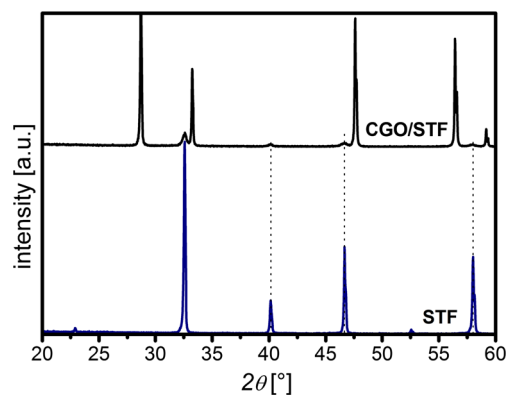


**Fig. 4** XRD patterns of the bulk STF and the STF thin layer deposited on a CGO substrate and annealed at 1100 °C (dotted vertical lines match the peaks corresponding to the bulk and thin layer STF)

proved that LNF, LSCF, and STF films have the same crystallographic structure as bulk materials. Figure 2 shows XRD patterns for the bulk LNF and the LNF layer deposited on a CGO substrate and annealed at 1100 °C. The observed reflections match the patterns, which were reported for the LNF and CGO compounds in Falcón et al. [29] and Zha et al. [30], respectively. Dotted vertical lines match the peaks corresponding to the bulk and thin layer LNF. No additional peaks were observed; thus, there are no secondary phases present in the layer within XRD sensitivity. Similarly, Fig. 3 shows XRD patterns for the bulk and thin film LSCF on CGO. Reflections observed for the bulk LSCF match the patterns reported in Tai et al. [25] and Kivi et al. [31]. Figure 4 shows the XRD diffraction patterns of the STF samples. The peaks observed for the bulk STF material are stronger than the ones observed for the other compounds. The reflections match the patterns, which were reported for the STF in Adler and Eriksson [32].

Deposited perovskite layers were visualized using AFM. The LSCF thin perovskite layer surface after deposition and

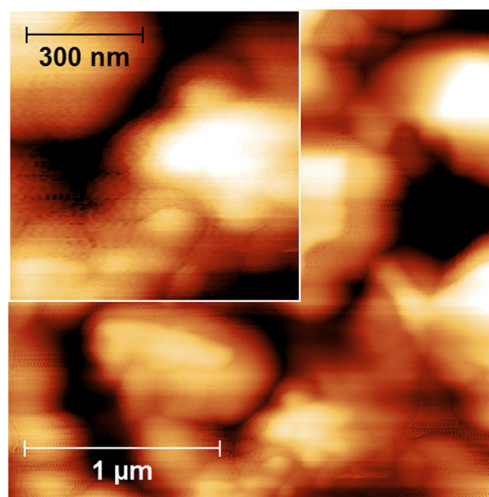


**Fig. 5** AFM micrograph of the LSCF thin layer surface fired at 500 °C. Inset shows magnification of grain-like structures

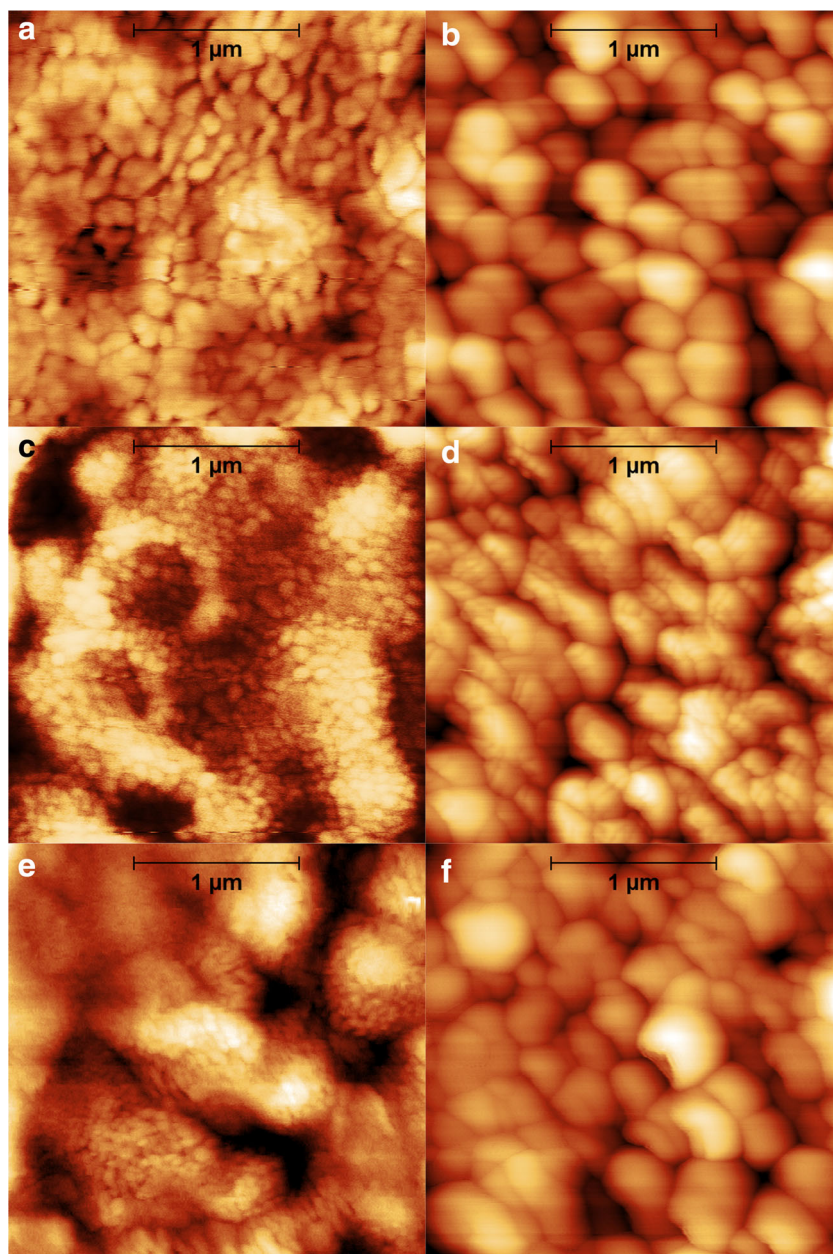
firing at 500 °C is shown in Fig. 5. There are some grain-like structures visible although they are not observed for the LNF and STF samples (not shown in this paper). These structures are magnified in the inset.

Figure 6 shows AFM surface micrograms of the LNF (Fig. 6a, b), LSCF (Fig. 6c, d), and STF (Fig. 6e, f) thin perovskite layers. Pictures on the left (Fig. 6a, c, e) show the structures annealed at 800 °C, while pictures on the right (Fig. 6b, d, f) show the structures annealed at 1100 °C (cathode sintering temperature). In case of the LNF layer annealed at 800 °C grain size is  $180\pm 14$  nm and increases up to  $290\pm 30$  nm once annealed at 1100 °C. The LSCF grains are smaller, i.e.,  $100\pm 30$  and  $205\pm 13$  nm once annealed at 800 and

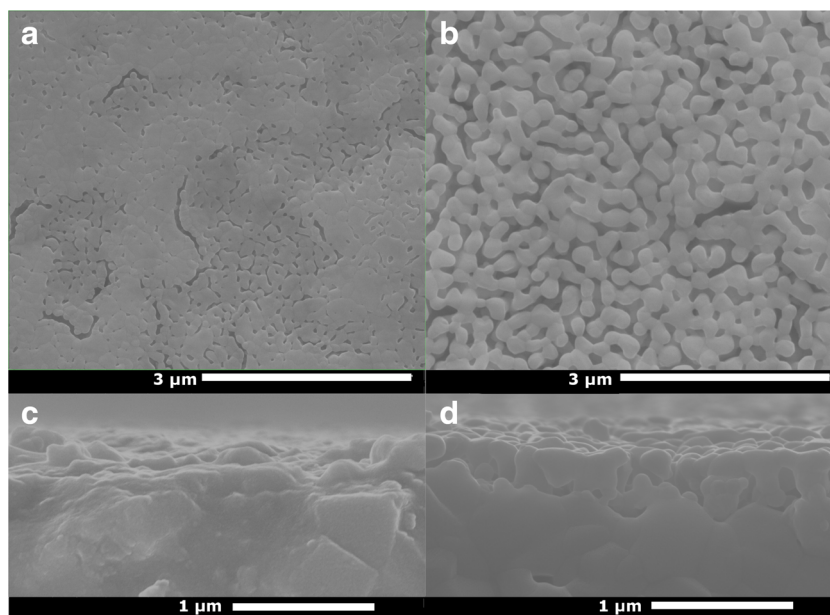
1100 °C, respectively. In the case of the STF layer annealed at 800 °C, the grains are hardly distinguishable—their mean size is  $70\pm 17$  nm, while for the layer annealed at 1100 °C, the grains grow up to  $230\pm 30$  nm. Clearly in the LNF layer, grain growth occurs faster than that in the other ones. It is also visible that the all studied samples annealed at 1100 °C have a well-defined microstructure.

Figures 7, 8, 9, and 10 show SEM images of the samples surfaces and cross sections. Figure 7a, b shows the surfaces, while Fig. 7c, d the cross sections of the LNF thin layers. The layer annealed at 800 °C (Fig. 7a, c) has a low amount of residual pores, and it is difficult to distinguish it from the CGO substrate. The coat covers the substrate with about

**Fig. 6** AFM micrographs of the thin perovskite layer surfaces. LNF annealed at **a** 800 °C, **b** 1100 °C; LSCF annealed at **c** 800 °C, **d** 1100 °C; STF annealed at **e** 800 °C, **f** 1100 °C



**Fig. 7** SEM micrographs of the LNF thin layer surface annealed at **a** 800 °C, **b** 1100 °C and cross section annealed at **c** 800 °C, **d** 1100 °C



190-nm-thick thin layer reproducing the substrate roughness. On the other hand, the layer annealed at 1100 °C (Fig. 7b, d) is clearly porous, and its structure is not determined by the substrate surface. As seen in the cross section, the layer is one to three grains thick (~300 nm) although it is not dense. The grain contact with CGO is well established. Figure 8 shows surface of LSCF layer after annealing at 800 °C (Fig. 8a) and 1100 °C (Fig. 8b). This layer is clearly denser than other two, after annealing at both 800 and 1100 °C, though there is some porosity visible in Fig. 8b. The STF layer after annealing at 800° and 1100 °C is shown in Fig. 9a, b, respectively. Its structure is similar to LSCF, although more pores are visible after annealing at 1100 °C.

Large residual pores which occurred after annealing are connected with a deterioration of the layers at relatively high sintering temperatures. This phenomenon is caused by faster clustering of crystallites than growth of crystallites itself [33, 34]. Furthermore, high temperatures induce grain spheroidization, which leads to cracks and pores when film

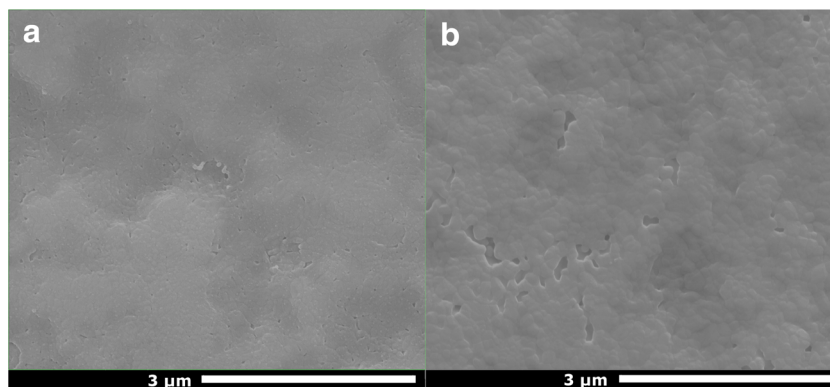
thickness is comparable or smaller than size of grains. Nevertheless, thin layers presented in this work adhere well to the CGO substrate, and no visual signs of delamination are observed.

Figure 10a, b shows the cathode-substrate interface without and with the (about 150 nm thick) LNF perovskite layer, respectively. As previously shown, the spin-coated layer annealed at 1100 °C is porous but exhibits a good contact with CGO. It is visible that the porous cathode deposited from the LNF paste without the thin perovskite layer has significantly smaller contact area. This may lead to the conclusion that depositing thin perovskite layer between cathode and substrate improves the contact area.

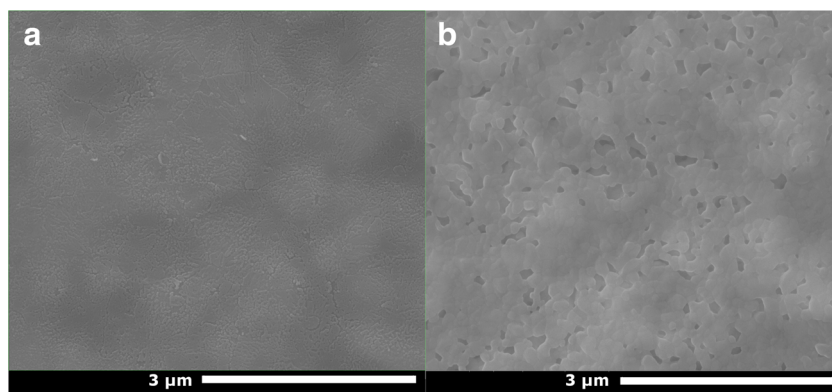
#### Electrical characterization of symmetrical cells

The symmetrical cathode/CGO/cathode cells were measured by means of electrochemical impedance spectroscopy. Introduction of the thin perovskite layer influences the

**Fig. 8** SEM micrographs of the LSCF thin layer surface after annealing at **a** 800 °C and **b** 1100 °C



**Fig. 9** SEM micrographs of the STF thin layer surface after annealing at **a** 800 °C and **b** 1100 °C



area-specific resistance (ASR). Examples of impedance spectra obtained at 800 °C for all four types of samples (without the thin perovskite layer and with the 160-nm-thin layers of LNF, LSCF, and STF) with the apparent ohmic resistance subtracted are shown in Fig. 11. It is clearly visible that the introduction of the LSCF and LNF layer decreased total polarization resistance in contrast to the STF layer. The simplest equivalent circuit should represent at least three relaxation processes at a high ( $10^4$  Hz), middle ( $10^2$  Hz), and low ( $10^0$  Hz) frequencies. However, the semicircles visible in the Nyquist plot are rather distorted, and the detailed analysis was not performed to avoid misinterpretations. Nevertheless, it can be noticed that the thin perovskite layer influences mainly the middle-frequency relaxation process, which is often associated with an interfacial resistance [35]. In

order to evaluate the correct model, further studies using a distribution of relaxation times method will be carried.

Figure 12 shows Arrhenius plots for all four types of samples, i.e., the sample without thin perovskite layer and three with layers spin-coated six times, which produced layers with thickness of approximately 160 nm. All samples except one with the STF layer demonstrate the ASR activation energy of 1.50 eV. The symmetrical cell with the STF thin perovskite layer has significantly higher activation energy, i.e., 1.68 eV. Such an increase indicates change in oxygen reduction reaction due to formation of a new, poorly catalytic, or nonconducting phase in the cathode/CGO interface or lower than LNF electronic conductivity of STF. Such a strong negative influence of STF itself is unlikely since it was shown to exhibit ASR values comparable to other cathode material like LSM or LNF [20] when deposited on YSZ electrolyte. Possibility of reaction between STF and LNF was subsequently confirmed by XRD analysis [36]. Introduction of the LSCF layer does not affect the activation energy, even though LSCF exhibits two orders of magnitude higher ionic conductivity than LNF. This indicates that such a thin layer does not significantly influence the oxygen reduction reaction mechanism.

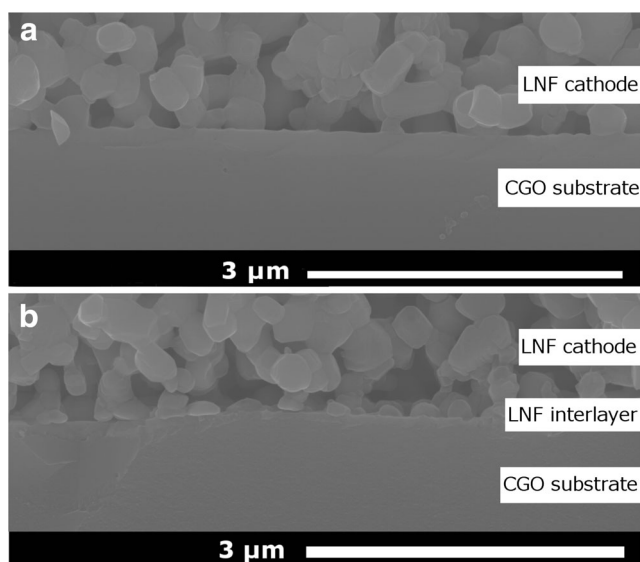


**Fig. 10** SEM micrographs of the cross section of a cathode-substrate interface without (a) and with (b) the LNF thin perovskite layer

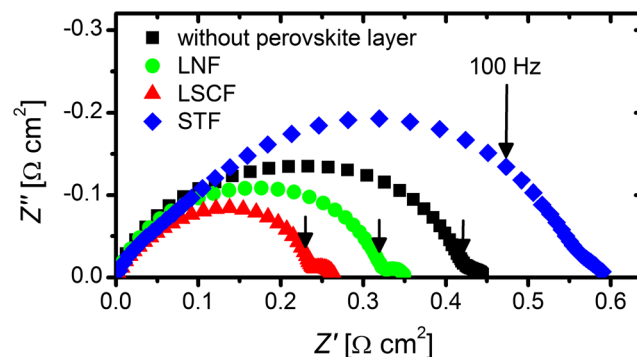


**Fig. 11** Typical impedance spectra obtained at 800 °C for structures without or with the 160-nm-thin perovskite layers

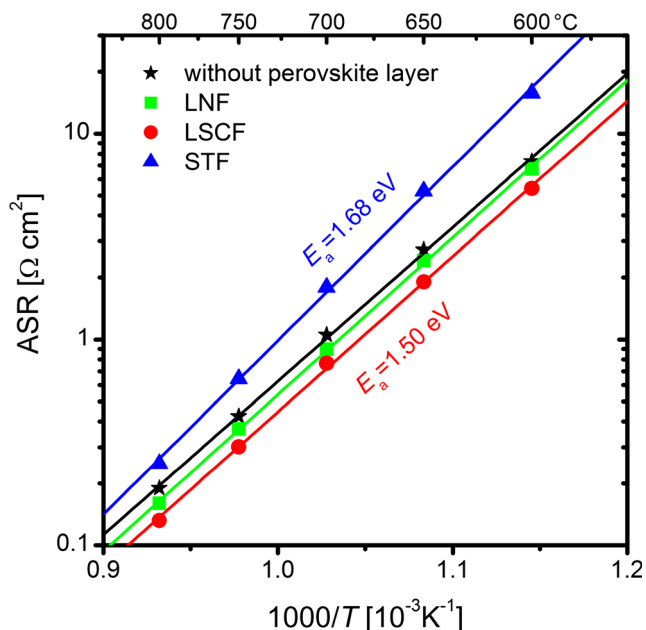


**Fig. 12** Arrhenius plot of the ASR for structures without or with the 160-nm-thin perovskite layers

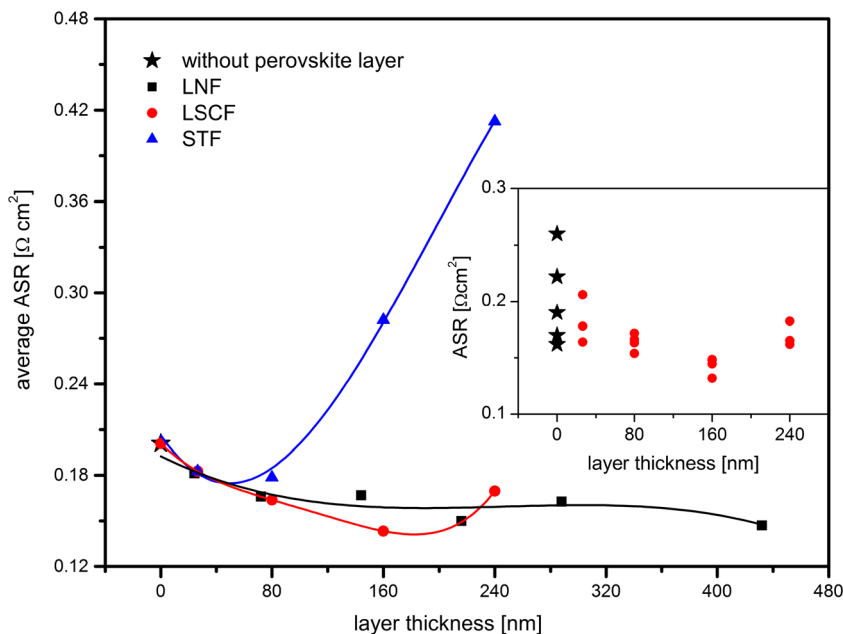
Figure 13 shows the average ASR for symmetrical cells at 800  $^{\circ}\text{C}$  as a function of the perovskite layer thickness (the marked thickness taken as-deposited). Multiple samples were measured for each thickness. Symmetrical cells without thin perovskite layer exhibit the average ASR of  $0.20 \Omega \text{ cm}^2$ . Apart from STF, the introduction of the thin perovskite layer lowers the average ASR with the minimum obtained for the 160-nm LSCF layer ( $0.14 \Omega \text{ cm}^2$ ). The inset shows single, not averaged measurements of

samples with LSCF layer or without any. It can be seen that minimal ASR of cathode without perovskite layer equals  $0.16 \Omega \text{ cm}^2$  which is a result comparable to systems with an additional layer; however, its reproducibility is poor. Distribution of ASR in the case of the samples with LSCF and LNF layer (LNF not shown) is significantly lowered which leads to conclusion that the introduction of the thin perovskite layer enables preparation of a more reproducible cathode-electrolyte contact. Introduction of 160-nm LSCF layer lowers minimal ASR to  $0.13 \Omega \text{ cm}^2$  with far greater consistency. Based on this and SEM images, it can be concluded that thin layer deposited by spin coating has much better contact with substrates and easily sinters with the later deposited porous cathode. The introduction of the layer thicker than 200 nm does not further improve the cathode/CGO interface. This supports the observation that the introduced thin perovskite layer improves a physical contact between the cathode and CGO, what results in the enhancement of the oxygen transfer mechanism through the interface without any change in the oxygen reduction reaction mechanism. In the case of the STF layer, the significantly higher ASR and low cathode reproducibility are observed. Increasing the thickness of STF layer increases the ASR, which supports conclusion that STF creates poorly catalytic phase.

**Conclusion**

In this paper, the influence of the spin-coated thin perovskite layer between an LNF cathode and a CGO substrate on the

**Fig. 13** The average ASR as a function of layer thickness for symmetrical cells at 800  $^{\circ}\text{C}$  (solid lines are a guide to the eye only). In the inset, individual ASR results of reproducibility measurements for sample without an additional layer and with LSCF thin layer



electrical properties of a symmetrical cells was investigated. Introduction of the LSCF layer improved the average area-specific resistance by 29 % at 800 °C. In the case of the  $\text{LaNi}_{0.6}\text{Fe}_{0.4}\text{O}_{3-\delta}$  layer, the average ASR was improved by 27 %. Important aspect of thin layer introduction was the increase of cathode resistance reproducibility, visible for layers with initial thickness above 80 nm. Based on SEM micrographs and the obtained activation energies of resistances, it was deduced that the thin perovskite layer improved the contact area and the oxygen ions transport between cathode and CGO without a significant change of the oxygen reduction reaction mechanism. The deposition of the approximately 160-nm-thin perovskite layers is particularly advised when the cathode sintering temperature is low, since at these temperatures, the adhesion between the cathode and an electrolyte is limited. In the presented investigation, the STF layer significantly increased the polarization resistance of the cells, which may be associated with its reaction with LNF.

**Acknowledgments** This work is partly supported by project founded by National Science Centre Poland based on decision DEC-2012/05/B/ST7/02153.

**Open Access** This article is distributed under the terms of the Creative Commons Attribution License which permits any use, distribution, and reproduction in any medium, provided the original author(s) and the source are credited.

## References

- Zhang X, Chan SH, Li G, Ho HK, Li J, Feng Z (2010) A review of integration strategies for solid oxide fuel cells. *J Power Sources* 195: 685–702
- Zhao Y, Xia C, Jia L, Wang Z, Li H, Yu J, Li Y (2013) Recent progress on solid oxide fuel cell: Lowering temperature and utilizing non-hydrogen fuels. *Int J Hydrog Energ* 38(36):16498–16517
- Ivers-Tiffée E, Weber A, Herbstreit D (2001) Materials and technologies for SOFC-components. *J Eur Ceram Soc* 21:1805–1811
- Tsipis EV, Kharton VV (2008) Electrode materials and reaction mechanisms in solid oxide fuel cells: a brief review. I. Performance-determining factors. *J Solid State Electrochem* 12: 1039–1060
- Tsipis EV, Kharton VV (2008) Electrode materials and reaction mechanisms in solid oxide fuel cells: a brief review. II. Electrochemical behavior vs. materials science aspects. *J Solid State Electrochem* 12:1367–1391
- Tsipis EV, Kharton VV (2011) Electrode materials and reaction mechanisms in solid oxide fuel cells: a brief review. III. Recent trends and selected methodological aspects. *J Solid State Electrochem* 15: 1007–1040
- Adler SB (2004) Factors governing oxygen reduction reaction in solid oxide fuel cell cathodes. *Chem Rev* 104:4791–4843
- Setevich CF, Mogni LV, Caneiro A, Prado FD (2012) Optimum cathode configuration for IT-SOFC using  $\text{La}_{0.4}\text{Ba}_{0.6}\text{CoO}_{3-\delta}$  and  $\text{Ce}_{0.9}\text{Gd}_{0.1}\text{O}_{1.95}$ . *Int J Hydrog Energ* 37:4895–4901
- McCoppin J, Young D, Reitz T, Maleszewski A, Mukhopadhyay S (2011) Solid oxide fuel cell with compositionally graded cathode functional layer deposited by pressure assisted dual-suspension spraying. *J Power Sources* 196:3761–3765
- Huang B, Zhu X, Nie H, Niu Y, Li Y, Cheng N (2013) Comparison of the electrochemical properties of impregnated and functionally gradient  $\text{LaNi}_{0.6}\text{Fe}_{0.4}\text{O}_3\text{-Gd}_{0.2}\text{Ce}_{0.8}\text{O}_2$  composite cathodes for solid oxide fuel cell. *J Power Sources* 235:20–28
- Haanappel VAC, Jordan N, Mai A, Mertens J, Serra JM, Tietz F et al (2009) Advances in research, development, and testing of single cells at forschungszentrum jülich. *J Fuel Cell Sci Technol* 6:021302
- Tanner CW, Fung KZ, Virkar AV (1997) The effect of porous composite electrode structure on solid oxide fuel cell performance. *J Electrochem Soc* 144(1):21–30
- Rieu M, Sayers R, Laguna-Bercero MA, Skinner SJ, Lenormand P, Ansart F (2010) Investigation of graded  $\text{La}_2\text{NiO}_{4+\delta}$  cathodes to improve SOFC electrochemical performance. *J Electrochem Soc* 157(4):B477–B480
- Woolley RJ, Skinner SJ (2014) Functionally graded composite  $\text{LaNiO}$  and  $\text{LaNiO}$  solid oxide fuel cell cathodes. *Solid State Ionics* 255:1–5
- Hildenbrand N, Boukamp B, Nammensma P, Blank D (2011) Improved cathode/electrolyte interface of SOFC. *Solid State Ionics* 192:12–15
- Hildenbrand N, Nammensma P, Blank DHA, Bouwmeester HJM, Boukamp BA (2013) Influence of configuration and microstructure on performance of  $\text{La}_2\text{NiO}_{4+\delta}$  IT-SOFC cathodes. *J Power Sources* 238:442–453
- Dumaisnil K, Fasquelle D, Mascot M, Rolle A, Roussel P, Minaud S et al (2014) Synthesis and characterization of  $\text{La}_{0.6}\text{Sr}_{0.4}\text{Co}_{0.8}\text{Fe}_{0.2}\text{O}_3$  films for solid oxide fuel cell cathodes. *Thin Solid Films* 553:89–92
- Stodolny MK, Boukamp BA, Blank DHA, van Berkel FPF (2011)  $\text{La}(\text{Ni}, \text{Fe})\text{O}_3$  stability in the presence of Cr species – solid-state reactivity study. *J Electrochem Soc* 158(2):B112–B116
- Jiang SP, Chen X (2014) Chromium deposition and poisoning of cathodes of solid oxide fuel cells—a review. *Int J Hydrog Energy* 39:505–531
- Molin S, Lewandowska-Iwaniak W, Kusz B, Gazda M, Jasinski P (2012) Structural and electrical properties of  $\text{Sr}(\text{Ti}, \text{Fe})\text{O}_{3-\delta}$  materials for SOFC cathodes. *J Electroceram* 28:80–87
- Niwa E, Uematsu C, Miyashita E, Ohzeki T, Hashimoto T (2011) Conductivity and sintering property of  $\text{LaNi}_{1-x}\text{Fe}_x\text{O}_3$  ceramics prepared by Pechini method. *Solid State Ionics* 201:87–93
- Morán-Ruiz A, Vidal K, Laguna-Bercero MÁ, Larrañaga (2014) A effects of using  $(\text{La}_{0.8}\text{Sr}_{0.2})_{0.95}\text{Fe}_{0.6}\text{Mn}_{0.3}\text{Co}_{0.1}\text{O}_3$  (LSFMC),  $\text{LaNi}_{0.6}\text{Fe}_{0.4}\text{O}_{3-\delta}$  (LNF) and  $\text{LaNi}_{0.6}\text{Co}_{0.4}\text{O}_{3-\delta}$  (LNC) as contact materials on solid oxide fuel cells. *J Power Sources* 248:1067–1076
- Montini T, Bevilacqua M, Fonda E, Casula MF, Lee S, Tavagnacco C, Gorte RJ, Fornasiero P (2009) Relationship between electrical behavior and structural characteristics in sr-doped  $\text{LaNi}_{0.6}\text{Fe}_{0.4}\text{O}_{3-\delta}$  mixed oxides. *Chem Mater* 21:1768–1774
- Ullmann H, Trofimenko N, Tietz F, Stöver D, Ahmad-Khanlou A (2000) Correlation between thermal expansion and oxide ion transport in mixed conducting perovskite-type oxides for SOFC cathodes. *Solid State Ionics* 138(1–2):79–90
- Tai LW, Nasrallah MM, Anderson HU, Sparlin DM, Sehlin SR (1995) Structure and electrical properties of  $\text{La}_{1-x}\text{Sr}_x\text{Co}_{1-y}\text{Fe}_y\text{O}_3$ . Part 2. The system  $\text{La}_{1-x}\text{Sr}_x\text{Co}_{0.2}\text{Fe}_{0.803}$ . *Solid State Ionics* 76:273–283
- Chourashiya MG, Bharadwaj SR, Jadhav LD (2010) Synthesis and characterization of electrolyte-grade 10%Gd-doped ceria thin film/ceramic substrate structures for solid oxide fuel cells. *Thin Solid Films* 519(2):650–657
- Chiba R, Tabata Y, Komatsu T, Orui H, Nozawa K, Arakawa M et al (2008) Property change of a  $\text{LaNi}_{0.6}\text{Fe}_{0.4}\text{O}_3$  cathode in the initial current loading process and the influence of a ceria interlayer. *Solid State Ionics* 178(31–32):1701–1709



28. Jasinski P, Molin S, Gazda M, Petrovsky V, Anderson HU (2009) Applications of spin coating of polymer precursor and slurry suspensions for solid oxide fuel cell fabrication. *J Power Sources* 194:10–15
29. Falcón H, Goeta AE, Punte G, Carbonio RE (1997) Crystal structure refinement and stability of  $\text{LaFe}_x\text{Ni}_{1-x}\text{O}_3$  solid solutions. *J Solid State Chem* 133:379–385
30. Zha S, Xia C, Meng G (2003) Effect of Gd (Sm) doping on properties of ceria electrolyte for solid oxide fuel cells. *J Power Sources* 115:44–48
31. Kivi I, Aruväli J, Kirsimäe K, Heinsaar A, Nurk G, Lust E (2013) Changes in LSC and LSCF cathode crystallographic parameters measured by electrochemical in situ high-temperature XRD. *ECS Trans* 57:1841–1849
32. Adler P, Eriksson S (2008) Structural properties, Mössbauer spectra, and magnetism of perovskite-type oxides  $\text{SrFe}_{1-x}\text{Ti}_x\text{O}_{3-y}$ . *Z Anorg Allg Chem* 626:118–124
33. Díaz-Parralejo A, Ortiz AL, Caruso R (2010) Effect of sintering temperature on the microstructure and mechanical properties of  $\text{ZrO}_2$ -3 mol% $\text{Y}_2\text{O}_3$  sol-gel films. *Ceram Int* 36:2281–2286
34. Oh EO, Whang CM, Lee YR, Lee JH, Yoon KJ, Kim BK, Son JW, Lee JH, Lee HW (2012) Thin film yttria-stabilized zirconia electrolyte for intermediate-temperature solid oxide fuel cells (IT-SOFCs) by chemical solution deposition. *J Eur Ceram Soc* 32:1733–17414
35. Baumann FS, Fleig J, Habermeier HU, Maier J (2006) Impedance spectroscopic study on well-defined  $(\text{La,Sr})(\text{Co,Fe})\text{O}_{3-\delta}$  model electrodes. *Solid State Ionics* 177:1071–1081
36. Chrzan A, Gazda M, Szymczewska D, Jasinski P (2014) Interaction of  $\text{SrTi}_{0.65}\text{Fe}_{0.35}\text{O}_{3-\delta}$  with  $\text{LaNi}_{0.6}\text{Fe}_{0.4}\text{O}_{3-\delta}$ ,  $\text{La}_{0.6}\text{Sr}_{0.4}\text{Co}_{0.2}\text{Fe}_{0.8}\text{O}_{3-\delta}$  and  $\text{Ce}_{0.8}\text{Gd}_{0.2}\text{O}_{2-\delta}$ . *Procedia Eng* 98:101–104